Induced tungsten melting events in the divertor of ASDEX Upgrade and their influence on plasma performance

K. Krieger, T. Lunt, R. Dux, A. Janzer, A. Kallenbach, H.W. Müller, R. Neu, T. Pütterich, V. Rohde and the ASDEX Upgrade Team

Max-Planck-Institut für Plasmaphysik, Garching, Germany

PACS: 28.52.Fa, 28.52.Nh, 52.25.Vy, 52.40.Hf, 52.70.Nc

JNM keywords: I0100, L0300, P0300, P0500, T1000

PSI19 keywords: ASDEX-Upgrade, Evaporation, Impurity screening, Liquid metal, Tungsten

Corresponding author address: Max-Planck-Institut f. Plasmaphysik, Boltzmannstr.2, 85748 Garching, Germany

Corresponding author email: krieger@ipp.mpg.de

Abstract

Tungsten rods of 1×1×3mm were exposed at the outer divertor plate of ASDEX Upgrade using a manipulator system. Controlled melting of the W rod in H-mode discharges was induced by moving the outer strike point towards the W-rod position. Visible light emission of ejected W droplets was recorded by fast camera systems. The resulting increase of tungsten concentration in the confined plasma was compared to that induced by W laser ablation into the outer main chamber boundary plasma. The resulting divertor retention expressed as ratio of tungsten core penetration probability from a divertor source to that of a main chamber source is ≈100. Ejected droplets are found to move always in general direction of the plasma flow. The measured magnitude of droplet acceleration shows that droplets are mainly subject to rocket forces and friction forces. Typical initial droplet size can be inferred from the time evolution of the droplet light emission to be $\geq 100\,\mu$m.

1. Introduction

Tungsten will initially be used for the baffle structure and parts of the divertor plates in the ITER divertor because of its favourable sputtering resilience and thermo mechanical properties. Safety limits with respect to tritium retention require an extension to a full tungsten divertor in later phases with pure D and D-T plasma operation. Off-normal transient heat loads in the divertor are expected to cause surface melting of tungsten armour. Detachment of melt layers will in turn eject tungsten into the divertor plasma fan in form of molten W droplets. Apart from surface damage issues, which are not discussed here, the key questions connected to W droplet ejection are on the one hand, what fraction of the ejected molten material will become ionised and on the other hand, on which characteristic time scale this process will occur. Furthermore, the resulting W leakage to the confined plasma is of critical importance for the performance and safety of plasma operation. While there are data available on divertor retention of tungsten [1], there are no experimental studies yet on the behaviour of liquid tungsten ejected into the divertor plasma. First experiments of this kind performing controlled tungsten melt events in the divertor of ASDEX Upgrade will be described in the following.

2. Experimental setup and procedure

For the controlled tungsten melting experiments a probe head equipped with a W-pin of 1×1 mm^2 cross-section and protruding 3mm above the plasma facing surface was constructed for the ASDEX Upgrade divertor manipulator system (Fig. 1). The probe exposure position is located at the outer divertor target plate. Local plasma flux and temperature and local power flux are measured by flush mounted Langmuir probes [2] and a thermography camera system [3] respectively. In addition spectroscopy of local line emission in the visible range is possible by optical fibres viewing the sample surface from below the dome baffle [1]. The W-pins

were exposed to H-mode discharges with plasma current $I_p = 0.8\,\mathrm{MA}$, toroidal field $B_t = -2.5\,\mathrm{T}$, average density $\bar{n}_e = 6.5\times10^{19}\ \mathrm{m}^{-3}$ and neutral beam heating powers of $P_{NBI} = 5\,\mathrm{MW}$ and 10MW respectively. In addition, central W concentration was controlled by electron cyclotron resonance heating with $P_{ECRH} = 1\,\mathrm{MW}$. Before the onset of auxiliary heating the outer strike point (OSP) was shifted $\approx 10\,\mathrm{cm}$ below the W-pin position. Melting of the pin was initiated by moving the strike point upwards to $\approx 3.5\,\mathrm{cm}$ below the W-pin position (Fig. 2). The sweep of the plasma across the installed Langmuir probes was also used to obtain spatial profiles of $\Gamma_{i,\|}$ and T_e at the outer target plate. Assuming a sheath transmission coefficient of ≈ 7.5 the parallel power flux at the pin location averaged over the time scale of ELM repetition ($\Delta t_{ELM} \approx 8\,\mathrm{ms}$) was estimated to $\bar{q}_{\|} \approx 60\,\mathrm{MW\,m^{-2}}$.

Because the melting pin was expected to eject W droplets into the plasma, a fast visible range camera system (frame rate either 10000 fps or 20000 fps) was installed, viewing vertically down to the exposure position (Fig. 1) with a viewing field spanning approximately 3 of the 16 toroidal sectors of the vessel. To improve contrast of the droplet light emission against the bright plasma background light in the divertor, the cameras were equipped with an H_α/H_β rejection filter.

3. Experimental results

Time traces of global plasma parameters as well as of OSP position and tungsten main plasma concentration are shown in Fig. 2 for the W-pin exposure in plasma discharge #25514. The onset of the W-pin melt events are clearly visible by the transient rise of the tungsten plasma concentration from $c_W \approx 2\times10^{-5}$ to $c_W \approx 4\times10^{-5}$ for $t \geq 2.1\mathrm{s}$. By weighing of the W-pin pre- and post-exposure including re-solidified residue at the sample surface, the total amount of lost molten mass was determined. Typical mass loss was 10-20 mg (20.6 mg in #25514

discussed here in detail). To determine the divertor screening of tungsten atoms originating from the ejected droplets, one needs the residence time of the droplets in the divertor plasma as well as the fraction of atoms released to the plasma by evaporation. Estimates of both quantities were obtained by analysis of the fast camera video recordings. The fast camera shows ejection of single droplets from the pin location, which always move in plasma downstream direction. However, their trajectory does not generally follow the B-field lines but has also often components directed radially outward and vertically upward. This might be an indication of droplets being ripped from the melting tip by the Lorentz force resulting from the interaction of thermal electron emission current and magnetic field. Fig. 3 shows an example for the time evolution of the visible light intensity emitted by an ejected droplet. The observed intensity bursts are correlated to respective ELMs. Typical lifetimes after which the droplets vanish are $\approx 0.1\,\mathrm{s}$. The three-dimensional position of the droplets cannot be determined from a single camera observation point. However, taking into account that the vertical component of the particle trajectories is typically $\ll$ their horizontally travelled distance, one can compute the distance *s* from the W-pin as function of time by projecting the line of sight between camera observation point and droplet into the horizontal plane through the W-pin. The example of *s(t)* for an ejected droplet shown in Fig. 4, shows that within the 0.1 s lifetime the droplets move by total distances of typically $\approx 2\,\mathrm{m}$, with a resulting average acceleration of $\approx 400\,\mathrm{ms}^{-2}$. Taking the second time derivative of *s(t)* reveals, however, a continuously decreasing acceleration.

4. Droplet lifetime and divertor screening

From the observed typical lifetime of ejected droplets, their approximate size can be derived by a simple model of droplet evaporation due to the incident power flux from the plasma. We assume that the droplets are so small that they are in thermal equilibrium. Hence the power

flux $q_{\|}$ received from the plasma is balanced by power loss due to thermal radiation and tungsten evaporation:

$$\frac{1}{2} q_{\|} = \Gamma_{vap} \frac{\Delta H_{vap}}{N_A} + \varepsilon_T \sigma T^4 \tag{4.1}$$

with the evaporation flux $\Gamma_{vap} = p_{vap} \Big/ \sqrt{2\pi m_W k_B T}$ where m_W is the tungsten atomic mass and the tungsten vapour pressure at temperature *T* is given by a Clausius-Clapeyron relation to the vapour pressure $p(T_m)$ at tungsten melt temperature T_m [4]

$$p_{vap} = p(T_m) e^{-\frac{\Delta H_{vap}}{N_A k_B}\left(\frac{1}{T} - \frac{1}{T_m}\right)}.$$

The power loss by W evaporation is then determined by the specific evaporation heat per atom [4] $\Delta H_{vap} / N_A = 824\,\mathrm{kJ mol^{-1}} / N_A$. The radiation power loss from the droplet is given by the Stefan-Boltzmann law with $\varepsilon_T = 0.347$ being the total emission coefficient of tungsten with respect to a black body radiator [5]. Solving (4.1) numerically yields the droplet temperature as function of parallel power flux.

The droplet evaporation is given by the particle balance differential equation for the number of W atoms N_W in a droplet of radius *r*:

$$\frac{dN_W}{dt} = -4\pi r^2 \Gamma_{vap}(t). \tag{4.2}$$

Using $N_W = \rho_W \, r^3 4\pi / 3$ equation (4.2) transforms into

$$\frac{dr(t)}{dt} = -\frac{1}{\rho_W} \Gamma_{vap}(t) \quad \text{and hence} \quad r(t) = r\big|_{t=0} - \frac{1}{\rho_W} \int_0^t \Gamma_{vap}(t')\, dt'. \tag{4.3}$$

This means that at constant power flux and correspondingly constant droplet temperature the droplet radius decreases linearly with time. As the experiments show that typical lifetimes

$\tau \gg \Delta t_{ELM}$ one can approximate $\Gamma_{vap}(t)$ by the constant average over an ELM period, $\bar{\Gamma}_{vap} \doteq \Gamma_{vap}\left(T(\bar{q}_{||})\right)$, which allows to express τ as function of initial droplet mass $m|_{t=0}$

$$\tau = \frac{1}{\bar{\Gamma}_{vap}} \sqrt[3]{\frac{3}{4\pi} \frac{m|_{t=0}}{m_W} \rho_W^2} \,. \tag{4.4}$$

With $\bar{q}_{||} \approx 60\,\mathrm{MW\,m^{-2}}$ e.g. in #25514, the observed flight times are shorther than the minimum droplet lifetimes computed from the lost W-pin mass and number of ejected droplets. However, using (4.3) one can estimate the total number of W atoms evaporated from the droplets into the divertor plasma within their flight time to 20-40% of the tungsten lost from the pin.

This number can be used to obtain an estimate of the divertor screening factor. With a plasma volume of 14 m^3 the observed increase of the W concentration corresponds to $\approx 3.4\times10^{16}$ W atoms. With $\approx 0.3\times6.8\times10^{19}$ W atoms released by the droplets, one ends up with a divertor screening factor of 600, which agrees well with the value determined in earlier experiments [1]. By comparing divertor screening to that of a W source at the main chamber, one can also derive the divertor retention coefficient for tungsten. To this end, tungsten laser blow off was used at a later time point in the discharges with W-pin exposure. Ablation of $\approx 120\,\mu g \equiv 4\times10^{17}$ W atoms lead to a similar increase of W concentration as with the W-melt source in the divertor with a corresponding main chamber screening factor of 10, which is comparable to earlier observations where a screening factor of 25 was found [9]. The resulting divertor retention coefficient, defined as ratio of divertor screening to main chamber screening, is 60, which agrees well with first modelling efforts using the EMC3 code [6].

5. Forces on the W droplets

The magnitude and time dependence of the observed droplet acceleration allows to draw conclusions on the forces acting on the droplets and which of them dominate the droplet acceleration. Firstly, if one assumes the droplet acts as spherical capacitor with charge Q according to its floating potential against the surrounding plasma, one can derive the corresponding acceleration of a droplet with mass m and corresponding radius r by an electric field E in a plasma with electron temperature T_e to

$$\frac{F_{el}}{m} = \frac{QE}{m} \approx \frac{4\pi\varepsilon_0 r 3T_e E}{m_W \rho_W \, 4\pi/3\, r^3} = \frac{9\varepsilon_0}{m_W \rho_W} \frac{T_e E}{r^2}. \tag{5.1}$$

Furthermore, an inhomogeneous power flux to the droplet, e.g. from upstream and downstream directions inside the local flux tube, will lead to a net rocket force due to the correspondingly inhomogeneous droplet evaporation flux:

$$\frac{F_{rocket}}{m} = \Delta \frac{m_W \Gamma_{vap} \pi r^2 \sqrt{kT/m_W}}{m_W \rho_W \, 4\pi/3\, r^3}\Bigg|_{T^-}^{T^+} = \frac{3}{4\sqrt{2\pi} m_W \rho_W} \frac{p_{vap}(T^+) - p_{vap}(T^-)}{r} \tag{5.2}$$

with T^+ and T^- denoting the approximate droplet temperature at upstream and downstream facing surface respectively. Taking into account that in thermal equilibrium, $p_{vap}(T^+) - p_{vap}(T^-) \sim (T^+ - T^-) \sim r,$ one can infer that the rocket force does not depend on droplet size.

In addition to this force, the droplet is subject to a friction force with the plasma streaming around it, which, taking into account that the velocity of the droplet is negligible against the plasma velocity, can be approximated by the force due to the plasma pressure difference between the upstream and downstream facing side of the droplet. Because the velocity of the droplet is small compared to the plasma flow velocity, one can consider the droplet as an immobile material target in the plasma. Using the expressions derived in [7] for upstream and

downstream plasma density at the sheath edge of such a target, n_e^{us} and n_e^{ds} respectively (assuming $M = 0.4$ far away from the droplet):

$$\frac{F_p}{m} = \frac{\pi r^2 \overbrace{(n_e^{us} - n_e^{ds})(kT_e + kT_i)}^{\Delta P}}{m_W \rho_W \, 4\pi/3 \, r^3} \approx \frac{1}{4 m_W \rho_W} \frac{n_e (kT_e + kT_i)}{r}. \qquad (5.3)$$

Inserting typical values of $T_{e,i} = 20\,\mathrm{eV}$, $n_e = 5 \times 10^{19}\ \mathrm{m}^{-3}$, an electric field near the target plate surface due to the pre-sheath potential, $E = 1000\,\mathrm{V\,m}^{-1}$ and assuming a droplet with radius of 100 μm exposed to a power flux of $q_{\parallel} = 60\,\mathrm{MW\,m}^{-2}$, the resulting acceleration due to electrical forces would be 0.01 m/s^2, while for rocket and friction forces one obtains acceleration values of 96 m/s^2 and 42 m/s^2 respectively. While these results are in line with those of a previous analysis on the dynamics of dust particles in the plasma boundary [8], the total acceleration derived from the computed force contributions is about a factor 3 smaller than the measured average acceleration (section 2). Taking into account the uncertainties in the values of plasma temperature, droplet size and temperature gradient inside the droplets assumed for the force computations, one still can conclude that rocket and friction forces dominate the droplet motion. However, as droplet size will decrease with time due to evaporation, the scaling of the different contributions to the droplet acceleration implies an acceleration increasing with time, opposite to the observed behaviour. This might be explained by the droplets' trajectories leading into colder plasma regions away from the separatrix with consequently decreasing friction and rocket force. The absence of any ELM effect on droplet acceleration, as shown by the smooth evolution of $s(t)$ in Fig. 4 indicates that the time period in which an ELM burst is passing the droplets in the boundary plasma is so small that the corresponding effect on the dominant friction and rocket forces is negligible. One should take into account that this conclusion might not hold anymore in the case of larger ELM power densities as expected e.g. in ITER. Therefore both the effects of transient

excursions from the stationary (inter ELM) boundary plasma conditions and the effects of spatial gradients of the plasma parameters on melt droplets must be included in a quantitative model for extrapolation to droplet propagation and evaporation under ITER-like conditions.

6. Conclusions

Controlled tungsten melting experiments were for the first time carried out in a divertor tokamak with ITER relevant geometry and boundary plasma conditions. After heating a W-pin exposed at the outer target plate to melting temperature of tungsten, ejection of molten tungsten droplets was observed with typical lifetimes of 0.1 s and flight path lengths of O(1 m). The scaling of both lifetime and droplet acceleration with droplet size at the given local plasma parameters show that ejected droplets have initially a typical size of O(100 μm). For plasma parameters typical for inter-ELM phases there are no fundamental differences to be expected in ITER. However, this conclusion might be incomplete, firstly due to the influence of the much higher expected ELM power and particle flux and the longer ELM repetition time in ITER, which are not accounted for in this analysis and secondly due to differences in divertor retention, where extrapolation based on current experiments is still subject to large uncertainties considering that modelling of these experiments is still an emerging activity.

References

[1] A. Geier et al., Plasma Phys. Control. Fusion **44** (2002) 2091.

[2] M. Weinlich et al., Europhysics Conference Abstracts (Proceedings of the 23rd EPS Conference on Controlled Fusion and Plasma Physics), Kiev, 1996, European Physical Society, Vol. 20 G/Part II, pp. 715–718.

[3] A. Herrmann et al., Plasma Physics and Controlled Fusion **37** (1995) 17.

[4] E.R. Plante et al., J. of Research of the Nat. Bureau of Standards **77A** (1973) 237.

[5] R. Allen et al., J. Appl. Phys. **31** (1960) 1382.

[6] T. Lunt et al., this conference.

[7] T. Lunt et al., Plasma Phys. Control. Fusion **49** (2007) 1783.

[8] S. I. Krasheninnikov et al., Physics of Plasmas **11** (2004) 3141.

[9] R. Neu et al., J. Nucl. Mat. **290-293** (2001) 206.

Figure captions

Figure 1: Poloidal cross-section through the ASDEX Upgrade vessel with manipulator systems and plasma configuration used in the stationary phase of the W-pin melt experiments.

Figure 2: Time traces of global discharge parameters, outer strike point position at the target plate and tungsten main plasma concentration in discharge #25514.

Figure 3: Intensity of visible light emission from a typical W-droplet recorded in #25514. Intensity was obtained by integrating a 3×3 pixel area centred at the droplet. H_α and H_β lines of recycling deuterium were suppressed by a rejection filter.

Figure 4: Distance travelled as function of time for the same droplet as recorded for the emission intensity data shown in Fig. 3. The distance was calculated by projecting the droplet position in the camera image to the horizontal plane of the W-pin location and integration of the path integral in this plane.

Figure 1

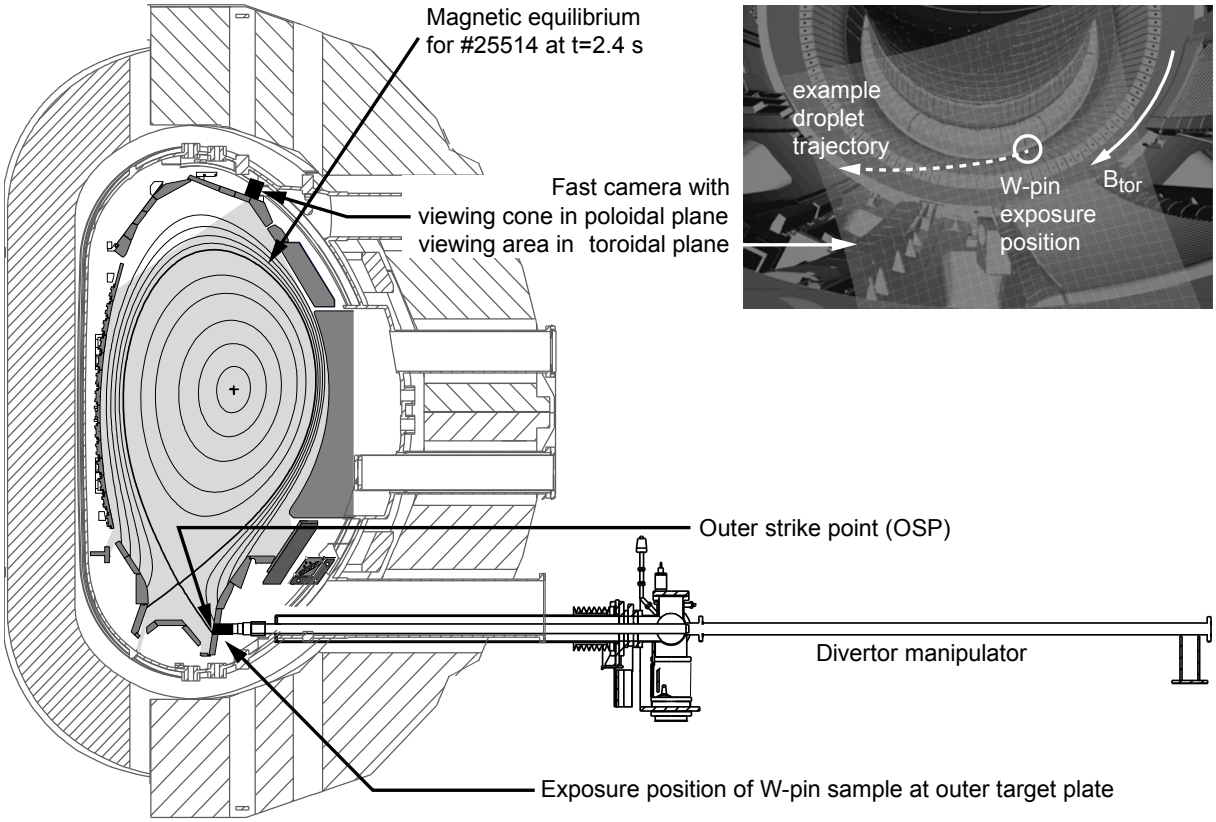
Magnetic equilibrium
for #25514 at t=2.4 s
Fast camera with
viewing cone in poloidal plane
viewing area in toroidal plane
example
droplet
trajectory
W-pin
exposure
position
B_{tor}
Outer strike point (OSP)
Divertor manipulator
Exposure position of W-pin sample at outer target plate

Figure 2

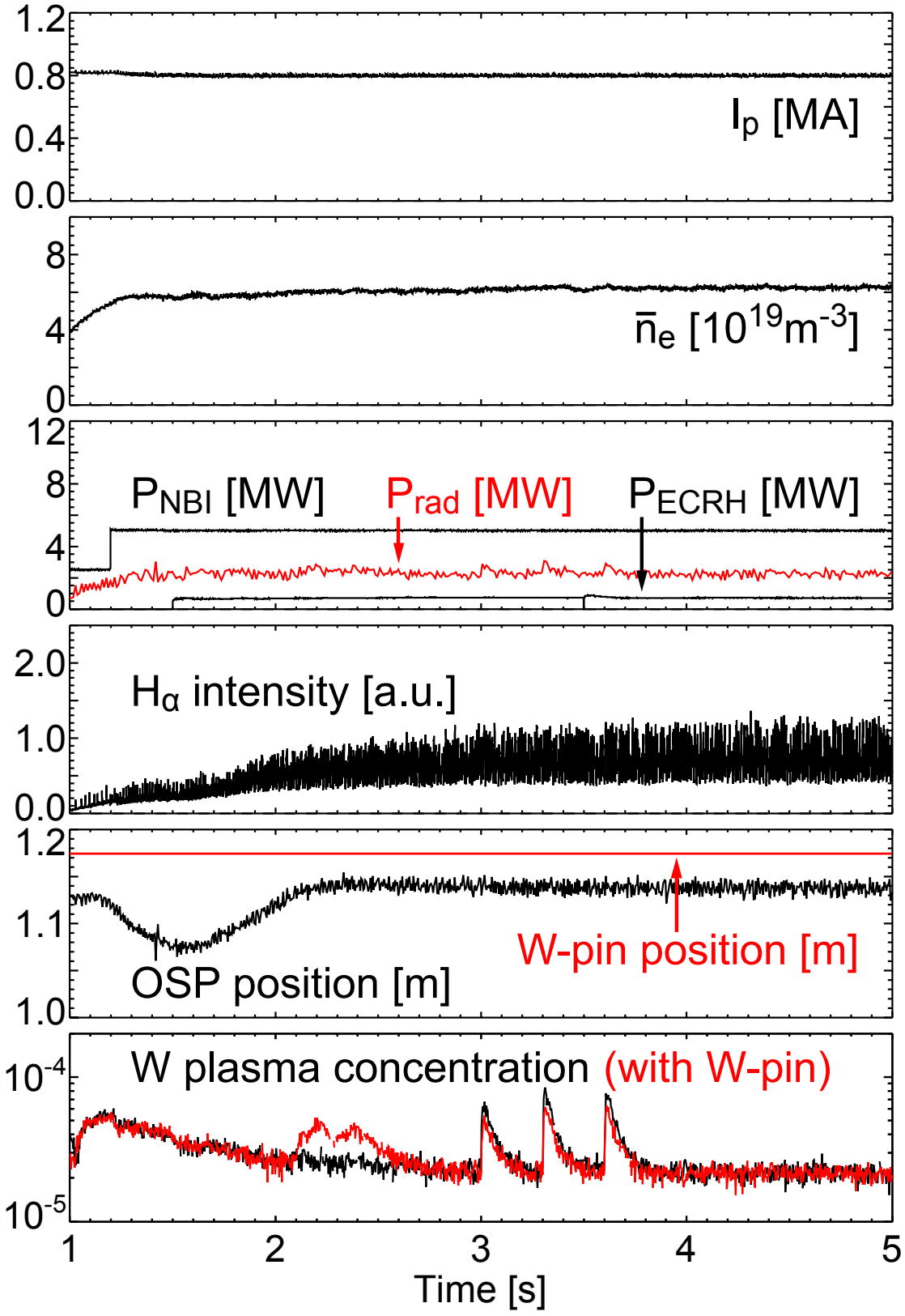
1.2
0.8
0.4
0.0
I_p [MA]
8
4
0
$\bar{n}_e$ [10^{19}m^{-3}]
12
8
4
0
P_{NBI} [MW]
P_{rad} [MW]
P_{ECRH} [MW]
2.0
1.0
0.0
H_α intensity [a.u.]
1.2
1.1
1.0
OSP position [m]
W-pin position [m]
10^{-4}
10^{-5}
W plasma concentration (with W-pin)
1
2
3
4
5
Time [s]

Figure 3

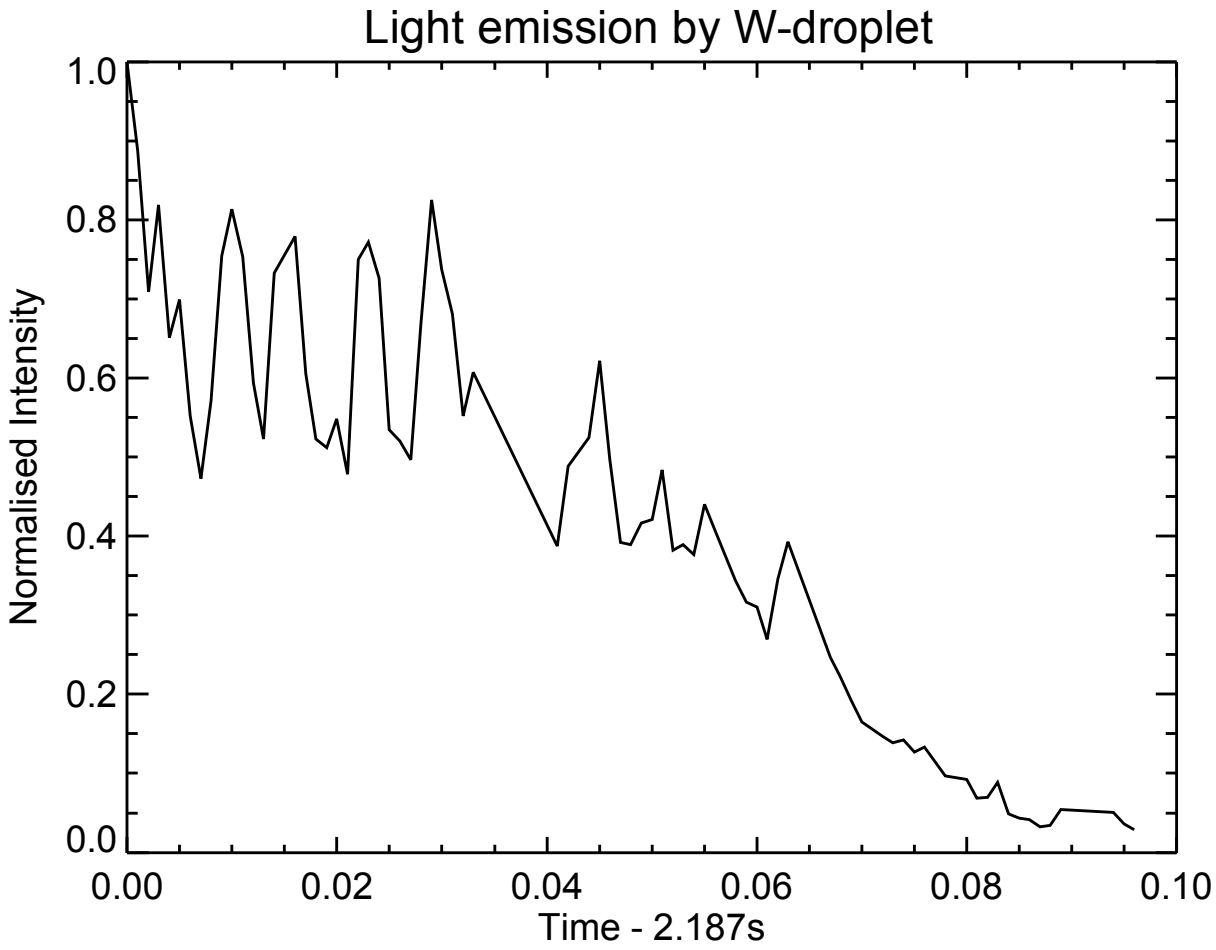
Light emission by W-droplet
Normalised Intensity
1.0
0.8
0.6
0.4
0.2
0.0
0.00
0.02
0.04
0.06
0.08
0.10
Time - 2.187s

Figure 4

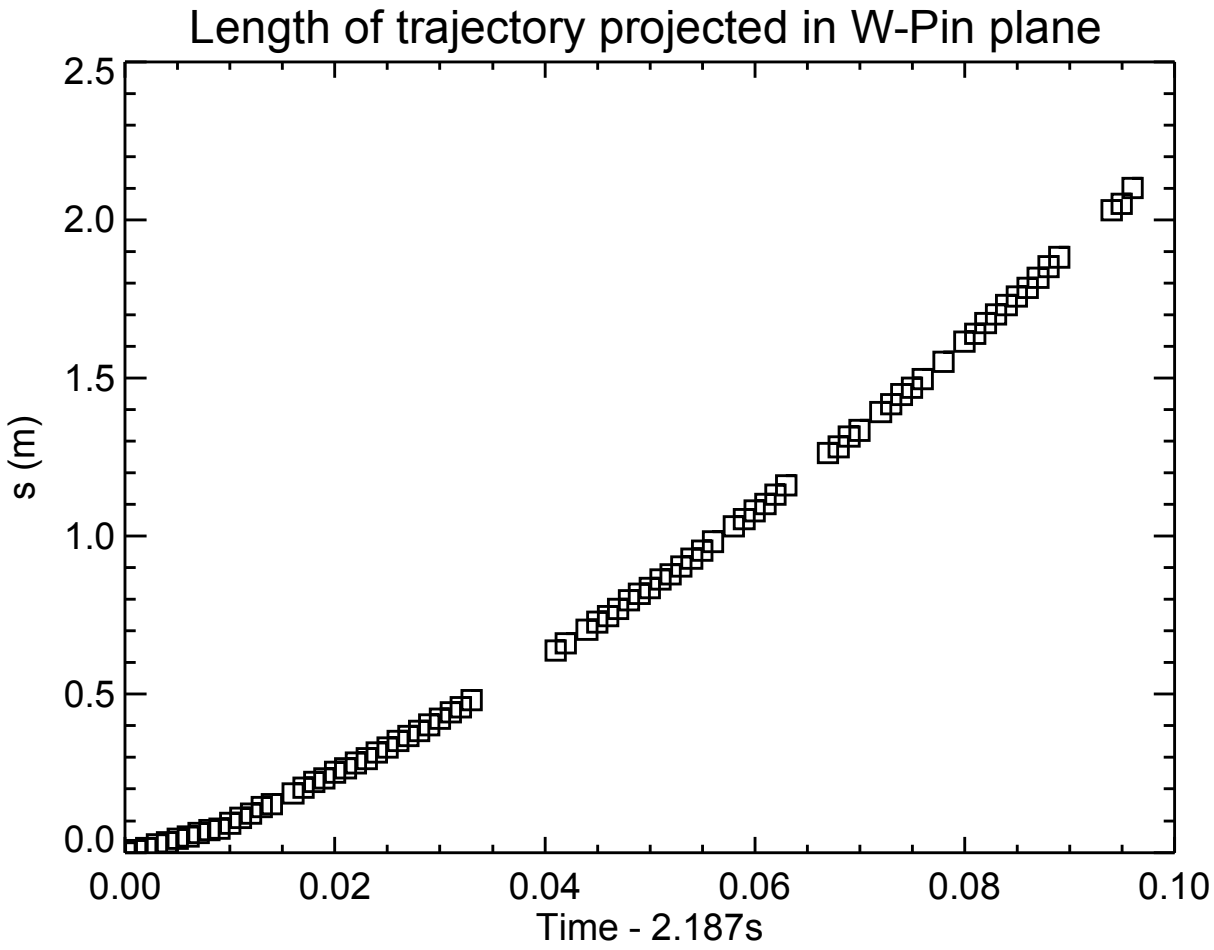
Length of trajectory projected in W-Pin plane
s (m)
2.5
2.0
1.5
1.0
0.5
0.0
0.00
0.02
0.04
0.06
0.08
0.10
Time - 2.187s